sustainability

MDPI

Article

Blast-Resistant Performance of Steel Petrochemical Control Room with 3D-Kagome Sandwich Wall

Zhijun Li *, Xinlong Dong, Dou Chen, Yan Jiang and Xuehua Li

School of Civil & Architecture Engineering, Xi'an Technological University, Xi'an 710021, China; dxlwalker923@gmail.com (X.D.); chendou555@sina.com (D.C.); yanyan20010311@163.com (Y.J.); xhli0724@163.com (X.L.)
* Correspondence: lzjsjh@aliyun.com

Abstract: As the control brain of the petrochemical plant, blast-resistant performance requirements are important for the sustainability of the petrochemical control room and should be guaranteed when the vapor cloud explosion occurs in the petrochemical production process. The 3D-Kagome truss core sandwich structure is a kind of blast-resistant material with high energy absorption and recycling. Considering the influential factors of the radius of the truss core rod and thickness of the upper and lower panels, in this paper, the blast-resistant performance of a real steel petrochemical control room with a 3D-Kagome truss core sandwich wall was analyzed. With the optimization goal of plastic deformation energy and panel displacement, the optimal wall thickness and radius of the truss core rod were obtained. The optimized blast-resistant walls were assembled, and the dynamic response of the steel petrochemical control room with the 3D-Kagome truss core sandwich blast-resistant wall was analyzed. The simulation results indicate that the truss core layer is ineffective in dissipating blast energy when the radius ratio of the truss core rod exceeds 2.7% of the total wall thickness. Moreover, as the thickness of the upper and lower panels increases from 0.5 cm to 3 cm, the proportion of plastic deformation energy in the truss core layer gradually rises from 55% to 95%, stabilizing at around 90%. The optimal configuration for blast resistance is achieved when the panel thickness ratio is 6.7% of the total wall thickness; the truss core rod radius ratio is 2.7% of the total thickness. This study establishes the effectiveness of the optimized 3D-Kagome sandwich wall as a blast-resistant solution for steel petrochemical control rooms.

Keywords: sustainability of petrochemical control room; 3D-Kagome; truss core sandwich wall; blast-resistant performance

Citation: Li, Z.; Dong, X.; Chen, D.; Jiang, Y.; Li, X. Blast-Resistant Performance of Steel Petrochemical Control Room with 3D-Kagome Sandwich Wall. *Sustainability* **2024**, *16*, 3967. https://doi.org/10.3390/su16103967

Received: 14 March 2024
Revised: 2 May 2024
Accepted: 7 May 2024
Published: 9 May 2024

1. Introduction

The petrochemical industry is the foundation for the development of various industries and has been developing rapidly in recent years. In petrochemical plants, the petrochemical control room is the center of the entire production process, controlling the operating status of the petrochemical plant and also serves as a gathering place for additional staff. In the current landscape, there is a noticeable trend towards larger, centralized, and more concentrated petrochemical plants. Unfortunately, this growth is accompanied by an escalating risk of explosion accidents, leading to severe consequences such as structural damage, casualties, and substantial economic losses [1]. An explosion at the Yeochun NCC (YNCC) plant in Yeosu, South Korea, resulted in four fatalities [2]. Similarly, the Shanghai petrochemical plant explosion led to multiple injuries and significant damage [3], and the Petronas Sabah-Sarawak gas pipeline explosion in Malaysia caused one fatality and two injuries [4]. These events, both recent and past, stress the urgent need to improve the blast resistance and energy absorption capabilities of the petrochemical control room structures. Given these ongoing risks, the sustainability development of innovative structural systems for the petrochemical control rooms is imperative.

Petrochemical control rooms typically require complex structural design specifications, including provisions for seismic, wind, and blast resistance. Additionally, these control rooms utilize high-strength and durable materials and must adhere to specialized design requirements, such as protection against chemical corrosion and the precise control of temperature and humidity. These factors contribute to differing structural responses and levels of damage between petrochemical control rooms and typical building structures when subjected to the same type of explosion. The Trinitrotoluene (TNT) equivalent method, representing the effects of vapor cloud explosions as TNT equivalents, is widely used in structural specifications [5,6] to facilitate the implementation of the design procedure. The ASCE (2010) Design Guide comprehensively addresses methods for predicting blast overpressure resulting from accidental explosions in petrochemical plants, along with quantifying the effects of such blasts on structures [7]. This guide offers blast-resistant design and structural reinforcement techniques to mitigate the hazards caused by unforeseen petrochemical explosions. Studies investigating damage to various structures caused by vapor cloud explosions have been conducted by the following researchers. Pritchard and Roberts [8] observed that the extent of damage to the structures depended on the distance from the center of the explosion. Clubley [9] performed full-scale experiments and finite element simulations to analyze the response of cylindrical shell structures subjected to high-power, prolonged explosions from sources such as hydrocarbon vapor clouds. Li et al. [10] examined the dynamic response of a reinforced concrete frame structure subjected to long-distance blast loading caused by an explosion, and their findings revealed that the cladding panels were particularly affected due to variations in blast forces acting on the structure. Blast-resistant walls, such as profiled/corrugated panels, are extensively utilized in the petroleum and gas industry to provide safety barriers against hydrocarbon explosions for personnel, facilities, and critical equipment on offshore platforms. The response of blast-resistant walls under hydrocarbon explosions has been extensively analyzed using nonlinear finite element models, and these findings were compared with design guidelines [11]. Furthermore, the response of steel-profiled blast barriers without passive impact barrier systems and with passive impact barrier systems placed at specific offset locations behind the blast barriers under hydrocarbon explosions has been investigated [12]. Additionally, in scenarios involving terrorist attacks and accidental explosions in the petrochemical industry, the corresponding studies have shown that protective walls or barriers are effective in minimizing blast effects and building damage [13]. Kiakojouri and his colleagues' research [14,15] emphasizes the potential impact of progressive collapse on structures. They particularly focus on the pivotal role of strengthening and retrofitting techniques in mitigating such collapses while also examining several parameters, including structural topology, the nature of triggering events, the initial collapse scale, collapse types, and seismic design requirements, and their influence on strengthening strategies.

Existing technologies for enhancing blast resistance in petrochemical control rooms mainly involve increasing the size of traditional reinforced concrete walls and columns. However, this conventional approach poses several challenges, especially in terms of cost-effectiveness and feasibility. Enlarging walls and columns significantly raises project expenses and becomes difficult to implement within existing space constraints [16]. Conversely, the use of lattice sandwich structures is gaining popularity in the construction sector due to their numerous benefits, including cost-effectiveness, lightweight properties, and thermal insulation [17]. It is important to acknowledge that sandwich panels with metal cores might encounter accidental industrial blast loads during their operational lifespan [18]. Moreover, these sandwich panels have found widespread application in the aerospace, automotive, shipbuilding, defense industries, and others [19]. Hence, conducting a thorough investigation into the performance of these structural panels under blast loading becomes imperative [20]. The performance of lattice sandwich materials in response to blast loading is outstanding, and extensive studies have revealed several key advantages. Ashkan Vaziri et al. studied the deformation patterns of lattice sandwich structures under blast loading, including tensile deformation of the upper and lower pan-

els, plastic deformation of the sandwich rods, and shear deformation between the core rods [21]. Similarly, Nan et al. investigated the mechanical properties of pyramidal kokomatsu sandwich panels under impact loads, providing a comprehensive analysis of rod diameter, aspect ratio, the number of units, and plies, further showcasing the superiority of lattice sandwich materials [22]. Moreover, Guoqi Zhang et al. conducted experiments to evaluate the stress–strain curves and energy absorption mechanisms of a pyramidal truss sandwich structure composed of carbon fiber-reinforced polymer (CFRP) panels and an aluminum alloy core, demonstrating its excellent energy absorption performance [23]. The numerical study by Ubade Kemerli et al. verified the advantages of lattice sandwich materials, particularly highlighting the conjugate forced convective heat transfer effect in sandwich panels with Kagome truss cores [24]. Their findings indicated that adjusting the length and diameter of stubs significantly improved the pressure drop and Nusselt number of fractional sandwich materials [24]. Parametric studies further reinforced the excellent performance of the lattice sandwich materials. By modeling seven combinations of outer layer thickness in ANSYS Workbench Explicit Dynamics (v19.2), researchers evaluated the effects of continuous blast loading on sandwich panel performance. The results revealed that pyramidal lattice panels exhibited high energy dissipation capacity in all different configurations, achieving energy absorption ranging from 5% to 48% [25]. In summary, lattice sandwich materials offer great potential in the design of blast-resistant petrochemical control rooms, given their exceptional blast resistance, lightweight properties, superior thermal insulation, and remarkable energy absorption capabilities.

In recent years, significant advancements have been made in the field of blast-resistant design for petrochemical control rooms, yet substantial gaps remain. The current structural sustainability design strategies, while improving, still do not fully address potential hazards effectively, particularly in integrating innovative materials and structural configurations that meet the required blast-resistant performance for modern petrochemical facilities. Considering the influential factors of the radius of the truss core rod and thickness of the upper and lower panels, in this paper, the blast-resistant performance of a real steel petrochemical control room with a 3D-Kagome truss core sandwich wall was analyzed. The study included numerical modeling of the control room structure subjected to vapor cloud explosion loads, the optimal blast-resistant design of the 3D-Kagome sandwich blast-resistant wall, and dynamic response analysis of the control room structure. The study addresses these critical gaps by introducing a holistic design strategy that not only leverages the potential of 3D-Kagome truss core sandwich structures, known for their superior blast resistance but also integrates these materials into optimized structural configurations so as to ensure greater safety and structural sustainability.

2. Material and Methods

2.1. Geometry of 3D-Kagome Sandwich Panels

With the development of material manufacturing technologies, the truss lattice material, as a porous material, has received great attention from various fields due to its excellent multifunctional performances of lightweight, high strength, blast resistance, heat insulation, and sound absorption. Truss core sandwich panels are generally classified into the following three types: tetrahedral, pyramid, and 3D-Kagome. Among these, the 3D-Kagome sandwich panel outperforms the other two types on the aforementioned multifunctional performances [25,26]. Therefore, the 3D-Kagome truss core sandwich structure was chosen in this paper. The structural model of this truss core sandwich panel is shown in Figure 1, and it consists of three parts: the upper panel, the middle truss core sandwich, and the lower panel.

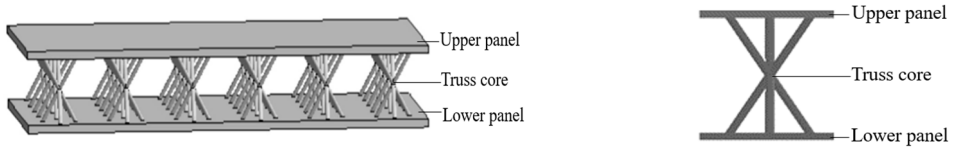

(**a**) (**b**)

Figure 1. 3D-Kagome sandwich structure: (**a**) 3D-Kagome truss core sandwich panel; (**b**) unit cell.

It is observed from Figure 1 that the 3D-Kagome truss core sandwich panel is constituted by the periodic arrangement of identical unit cells. The truss core of a unit cell structure is shown in Figure 2, in which B_c is the distance between different unit cells, H_c is the height of the sandwich layer, R_c is the radius of the truss core rod, $2L_c$ is the length of the truss core rod, and ω is the angle between the truss core rod axis and the upper/ lower panels.

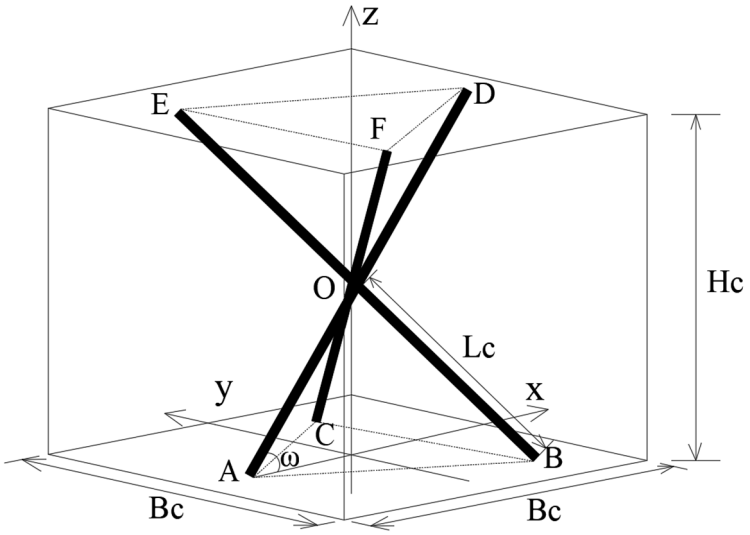

Figure 2. Truss core of unit cell.

The relative density is one of the important parameters for the 3D-Kagome truss core sandwich panel, which consists of the relative density of the truss core layer and ones of upper and lower sandwich panels. The relative density of the 3D-Kagome truss core sandwich panel is described by the following equations [27]:

$$\mathbf{sin}\omega = \frac{H_c}{2L_c} \tag{1}$$

$$\overline{\rho}_c = \frac{\rho_c}{\rho} = \frac{6\pi L_c}{H_c}\left(\frac{R_c}{B_c}\right)^2 = \frac{3\pi}{\sin\omega}\left(\frac{R_c}{B_c}\right)^2 \tag{2}$$

Substituting Equation (1) into Equation (2) transfer them to the following form:

$$\overline{\rho} = \frac{2hB_c^2 + 6\pi {R_c}^2 L_c}{(H_c + 2h)B_c^2} \tag{3}$$

where $\overline{\rho}$ is the relative density of the truss core of the unit cell, and h is the thickness of the upper and lower panels.

Under the blast load, the deformation of 3D-Kagome truss core sandwich panels mainly includes the tensile deformation of upper and lower panels, plastic deformation of the truss core layer, and shear deformation between the core layer and upper/lower panels [25]. The blast energy is mainly absorbed by the truss of the core layer.

2.2. Finite Element Method and Model Validation via Blast Experiments

It is very difficult to carry out the blast experiment for the real petrochemical control room with the 3D-Kagome truss core sandwich blast-resistant wall. The effective numerical computational method is presented in the manuscript for the analysis of the blast-resistant performance of the petrochemical control room authors based on the design code.

To simulate infinite space, the explosion shockwave can freely propagate at the air boundary. In the air model, except for the bottom surface, all other locations are set as non-reflective boundaries.

The finite element method (FEM) is widely used for structural analysis. In this method, the structure is divided into small elements, and the behavior of each element is analyzed. These elements are connected at points called nodes, forming a mesh. FEM is suitable for studying the dynamic behavior of structures subjected to various loads, including blast loads. For nodes in the finite element model, the connection (either welded or bolted) is simulated using the TIED contact keyword.

Based on the finite element method, a numerical model was constructed to faithfully replicate the geometric shape of the petrochemical control room. This encompasses the top, bottom, and potential additional structural elements, such as beams and panels. Key components of the structure, including steel frame beams and columns, were modeled with an H-shaped cross-section, utilizing Q235 as the material type.

In order to verify the accuracy of the explosion simulation method proposed in this paper, this section establishes a finite element analysis model based on the dynamics analysis software ANSYS/LS-DYNA (v19.2), and the real blast experiment of the pyramid sandwich panel provided by Ref. [28] is simulated. The size of the experimental sandwich panel shown in Figure 3 is 0.61 m × 0.61 m, and the surrounding of the panel is fixed with bolts, which results in an actual bearing load size of 0.41 m × 0.41 m. The blast distance is 150 mm above the center of the panel, and the amount of explosive is 150 g of the composition C-4.

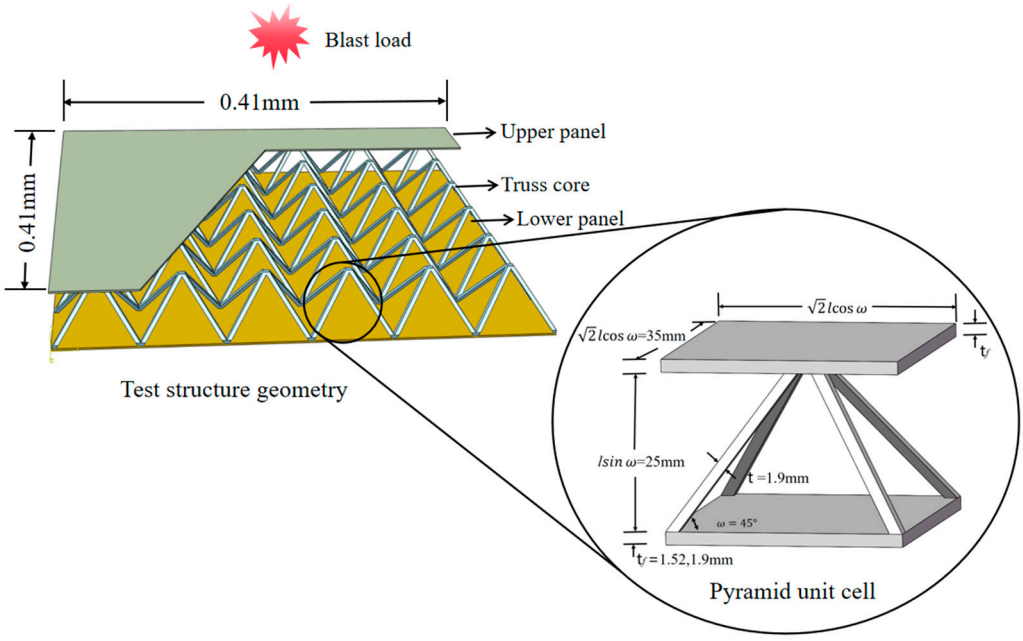

Figure 3. Test structure geometry.

In the numerical simulation, the panel and the core layer adopt the same material of AL6XN stainless steel. Considering the symmetry of the structure, the 1/4 model is used, and the symmetric constraint boundary conditions are set. The panel adopts a four-node shell element, and the core web is meshed by the solid element. The core body is defined as automatic single-sided contact, and the Contact_Tied_Surface_To_Surface contact is used

between the panel and the core body. Because the four sides of the plate are fixed by bolts and supported on the I-shaped bracket in the experiment, the constraint condition of the model is fixed on four sides. The displacement clouds of the finite element model subjected to the blast load are shown in Figure 4.

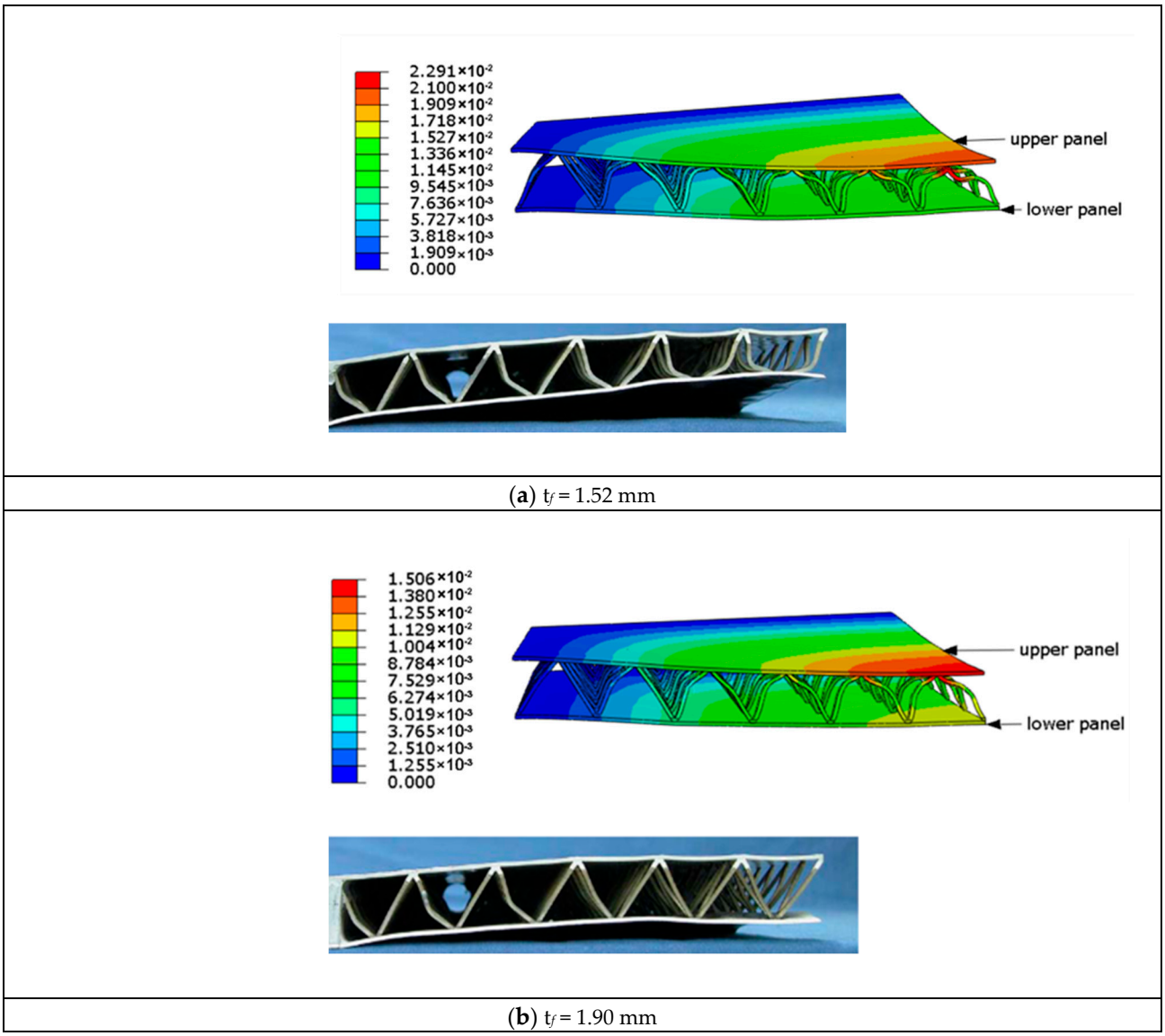

Figure 4. FEM and experimental samples for Pyramid sandwich panel under the blast load.

According to Table 1, the simulation results of the peak deflection of sandwich panels with different thicknesses under the blast load agree well with the experimental ones, and the errors are less than 10%, which verifies the effectiveness of the finite element model proposed in this paper.

Table 1. Comparison of peak deflection of sandwich panel.

	t_f = 1.52 mm		t_f = 1.90 mm	
	Upper Panel	**Low Panel**	**Upper Panel**	**Low Panel**
experiment [28]	21.72 mm	14.92 mm	14.51 mm	11.02 mm
simulation	22.91 mm	15.91 mm	15.06 mm	11.37 mm
error	5.48%	6.63%	3.79%	3.18%

In this study, the material model for structural steel was rigorously evaluated using another blast test conducted on the Q235 steel panel [29]. Each panel, sized 400 mm x 400 mm, was tested at thicknesses of 1.5 mm and 2 mm, securely bolted around the edges to ensure fixed boundary conditions. The test panel was subjected to TNT equivalents of 40 g and 60 g at a detonation distance of 50 mm, designed to mimic potential real-world blast scenarios that might affect the petrochemical control room. The displacement clouds of the finite element model subjected to the blast load are shown in Figure 5a–d.

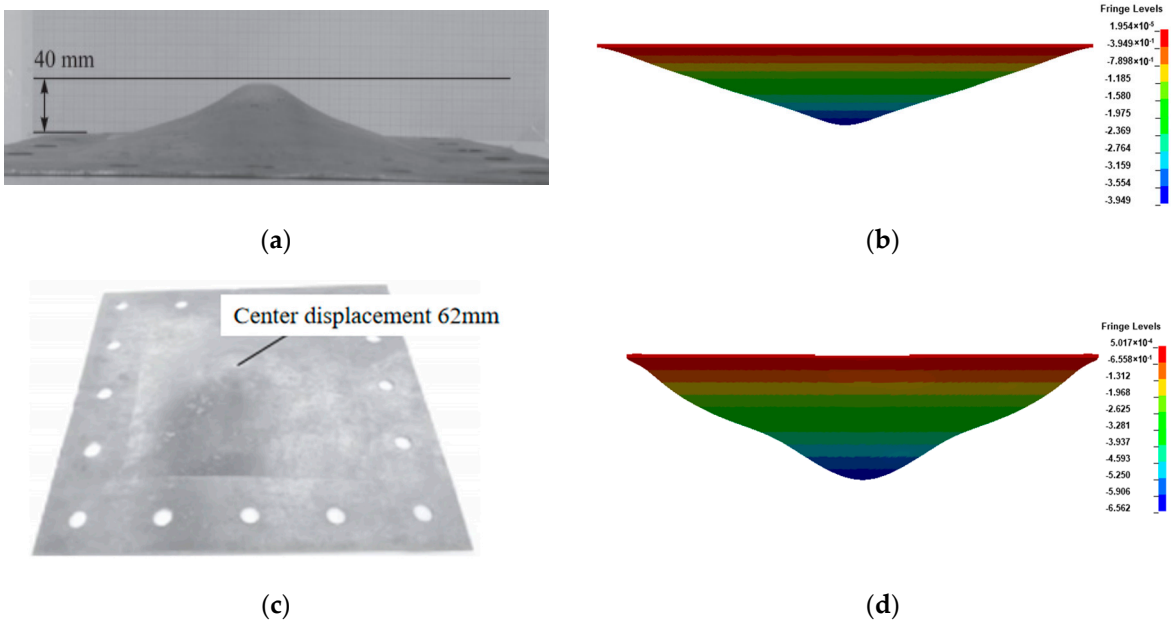

Figure 5. Comparison of simulated and experimental results of a steel panel with (**a**) experimental deformation of the 1.5 mm thick steel panel (TNT = 40 g), (**b**) simulated deformation cloud diagram of the 1.5 mm thick steel panel (TNT = 40 g), (**c**) experimental deformation of the 2 mm thick steel panel (TNT = 60 g), and (**d**) simulated deformation cloud diagram of the 2 mm thick steel panel (TNT = 60 g).

The results from these tests are described in Table 2, which compares the central displacements observed in the experiments with those predicted by the simulation models.

Table 2. Comparison of center point displacement of steel panel.

TNT/g	Experiment [29]	Simulation	Error
40 g	40.0 mm	39.5 mm	1.25%
60 g	62.0 mm	65.6 mm	5.8%

According to Figure 5a–d and Table 2, the simulation results of the center point displacement of steel panels with different thicknesses under the blast load agree well with the experimental ones, and the errors are less than 6%, which verifies the effectiveness of the material model used in the simulations.

2.3. Finite Element Model (FEM) of the Petrochemical Control Room Structure

To ensure the feasibility of the FEM of a real steel petrochemical control room with a 3D-Kagome truss core sandwich wall, the following simplifications were made:

(1) The impact of doors and windows on the blast load was not considered, and the structures were treated as fully enclosed.
(2) Interaction between the foundation and the upper structure of the petrochemical control room was not taken into account.
(3) Contact keywords were used to ensure that there was no relative sliding or separation at the connection points.

(4) The potential secondary effects of the explosion, such as fires, on the structure were not considered.

The real steel petrochemical control structure shown in Figure 6 is presented in this paper to testify to the blast-resistant performance of the new 3D-Kagome truss sandwich wall. The length of the structure is 35.7 m, the width is 27.0 m, and the height is 6.0 m. The main members of the structure, such as the steel frame beam and column, are chosen with the H section, and the cross-sectional size of each member is shown in Table 3.

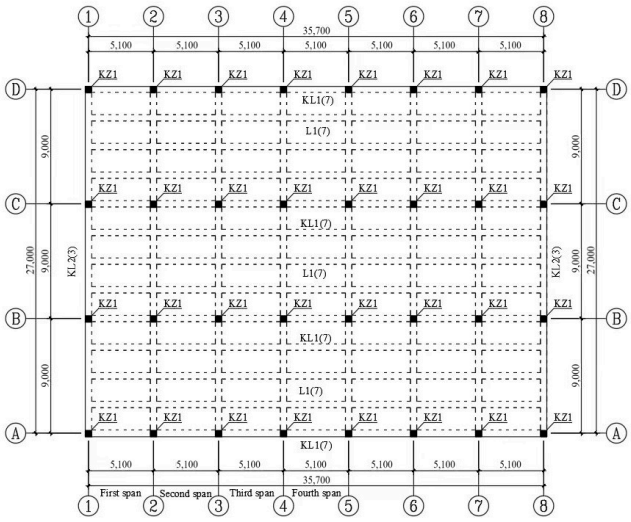

Figure 6. Plan of steel petrochemical control structure. (Numbers 1–8 are the vertical axis number and letters A–D are the horizontal axis number).

Table 3. Section sizes of the beam and column of the steel frame.

Type	Symbol	Cross-Section Size (mm)
Column (Q235)	KZ1	350 × 350 × 12 × 19
Beam (Q235)	KL1	700 × 300 × 13 × 24
	KL2	700 × 300 × 13 × 24
Reinforced concrete slab	L1	350 × 175 × 7 × 11
	RCC Slab	2000 × 1000 × 120

In Table 3, the cross-section size of each element is provided in millimeters (mm), and the dimensions represent the width, depth, flange thickness, and web thickness, respectively. For the column labeled 'Column (Q235)—KZ1', the dimensions '350 × 350 × 12 × 19' correspond to a cross-section with a width of 350 mm, a depth of 350 mm, a flange thickness of 12 mm, and a web thickness of 19 mm. Similar explanations are applied to the beam and reinforced concrete slabs.

The FEM of the steel petrochemical structure is shown in Figure 7, where all components of the structure are simulated using solid units; the diagram mainly illustrates the layout of the structural beams and columns in the control room, with the slabs hidden in the finite element model. Additionally, it should be noted that the petrochemical control structure model includes a perimeter of shear walls strategically placed around the structure for enhanced stability and resistance to lateral forces. The connection node (welded or bolted) between the structural column and main beam is depicted in Figure 8a, while the connection node between the main beam and secondary beam is shown in Figure 8b. In the simulation, the column foot condition is represented by fixed constraints, and all contact units are defined as "CONTACT AUTOMATIC SURFACE TO SURFACE".

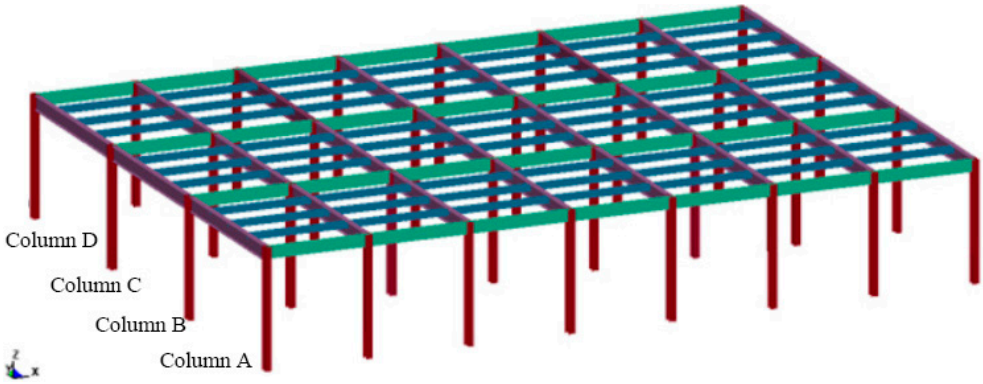

Figure 7. Structural model of petrochemical control room.

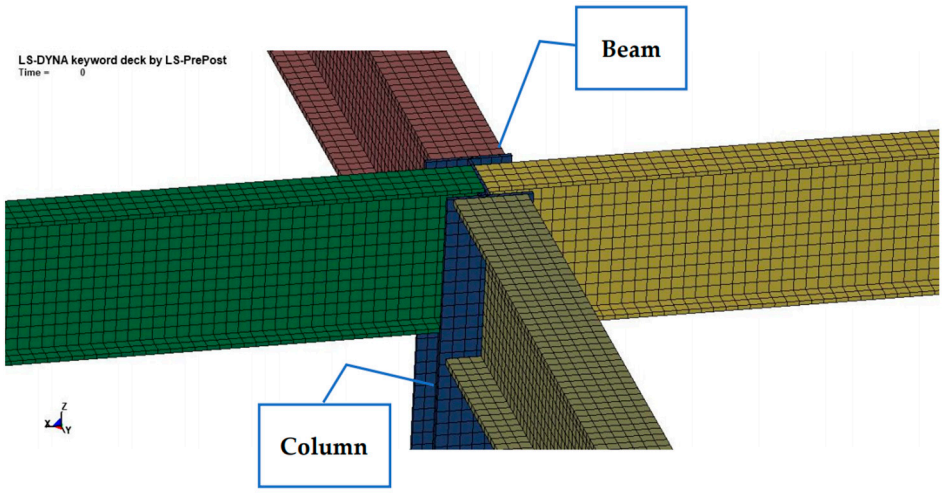

(**a**) Nodes between column and main beam.

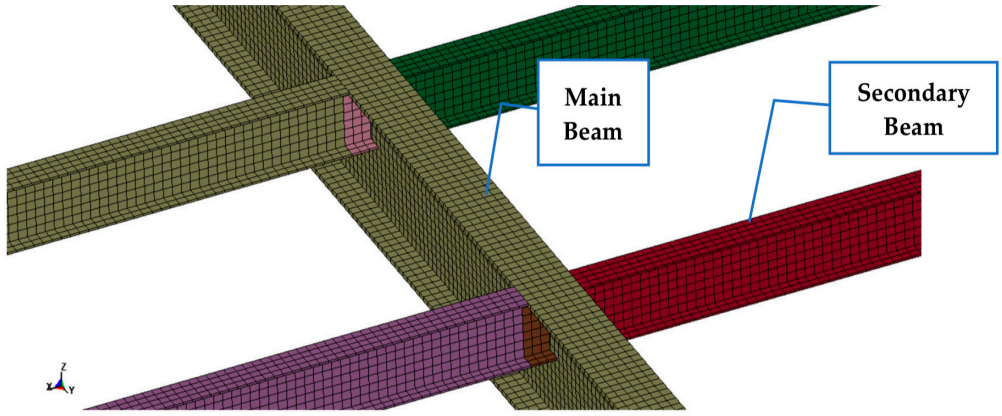

(**b**) Nodes between main beam and secondary beam.

Figure 8. The connection nodes.

Johnson and Cook (1983) [30] proposed a concise model to characterize the plastic response of metals subjected to dynamic loading. The model establishes a relationship between the equivalent flow stress and the variables of strain, strain rate, and temperature. The JC model is renowned for its versatility, broad applicability—especially under dynamic loading conditions—and ease of parameter calibration. The similarity between our materials and those research results successfully validated using the JC model provided a robust foundation for our implementation. Furthermore, the JC model strikes an optimal balance between accuracy and computational efficiency. In this paper, the Johnson–Cook

(J–C) material model and the GRUNEISEN state equation were used for the structure, and the yield stress of the structural steel was calculated according to Equation (4) [30]:

$$\sigma_y = (A + B\varepsilon^n)\left(1 + C_1 \mathbf{ln}\dot{\varepsilon}\right)\left[1 - (T_h)^M\right] \quad (4)$$

where A is the baseline yield strength, B is the hardening factor of the yield strength, n is the hardening exponent, ε^n is the effective plastic strain, $\dot{\varepsilon}$ is the strain rate, C_1 is the strain rate sensitivity coefficient, T_h is the reference temperature, and M is the temperature dependency index.

Johnson and Cook (1985) [31] expanded their basic model based on cumulative damage, and the LS-DYNA implementation of the Johnson–Cook constitutive model included this additional model feature. For the J-C failure model, the failure criterion is defined as follows:

$$\varepsilon^f = \left[D_1 + D_2 \mathbf{exp}(D_3 \frac{P}{\sigma_{eff}})\right](1 + D_4 \mathbf{ln}\dot{\varepsilon}^*)(1 + D_5 T_h) \quad (5)$$

where ε^f is the failure strain, P is the stress, σ_{eff} is the effective stress, $\dot{\varepsilon}^*$ is the plastic strain rate, and D_1, D_2, D_3, D_4, D_5 are the material parameters.

The GRUNEISEN state equation is described by [25] as follows:

$$p = \frac{r_0 C_s^2 m\left[1 + (1 - \frac{g_0}{2})m - \frac{\alpha}{2}m^2\right]}{\left[1 - (S_1 - 1)m - S_2 \frac{m^2}{m+1} - S_3 \frac{m^3}{(m+1)^2}\right]} + (g_0 + \alpha m)E_0 \quad (6)$$

where p is pressure, m is the compression ratio, r_0 is the initial material density, C_s is the speed of sound, g_0 is the Gruneisen parameter, α is the correction factor, E_0 is the internal energy, and S_1, S_2, and S_3 are the parameters of the state equation.

The parameters of the J-C model and the GRUNEISEN state equation are shown in Tables 4 and 5:

Table 4. J-C model parameters.

A	B	ε^n	C	M
8E8	4.5E8	0.565	0.067	1.03
T_h	D_1	D_2	D_3	D_4
1793	0.0705	1.732	−0.54	−0.015

Table 5. GRUNEISEN state equation parameters.

C_s	S_1	S_2	S_3	E_0
0.45	1.49	0.0	0.0	0.0

Avoiding the low efficiency of the traditional Arbitrary Lagrangian–Eulerian (ALE) algorithm for solving fluid–structure-coupled problems, the CONWEP blast load model is used in which the blast load is calculated by defining the TNT charge, explosion surface, explosion location, explosion time and explosion pattern.

3. Optimal Design of Blast-Resistant Shearing Wall with 3D-Kagome Sandwich Materials

According to the Code for the Design of Blast-Resistant Control Building in the Petrochemical Industry (GB50779-2012) [5], it is required that the blast-resistant structure has the ability to bear a shock overpressure wave with 69 kPa, which means the explosion with 1-ton TNT occurs in the center of the structure at the blast distance of 30 m. The width of the blast-resistant wall with a 3D-Kagome truss core sandwich structure is chosen as 1.5 m with reference to the Chinese building design standard (14J938) [6], and the length and

thickness of the blast-resistant wall are chosen as 5.1 m and 150 mm, respectively, according to the engineering background case.

The optimization design objectives of the blast-resistant wall with the 3D-Kagome truss core sandwich structure are the plastic deformation energy of the truss core of the sandwich layer and the maximum displacement out of the panel plan for the sandwich structure.

According to the Code for the design of blast-resistant control buildings in the petrochemical industry (GB50779-2012) [5], the deformation limits for the steel structural members are shown in Table 6.

Table 6. Deformation limits of steel structural members.

Structural Elements	Support Rotation (θ)
Main hot-rolled steel deck beam, secondary beam, and purlin	6°
Frame column, compression brace	1.5°
Frame beam, tensile brace	2°
Steel slab	6°
Lattice beam	3°
Cold-formed light steel panel (fixed end)	2°
Cold-formed light steel panel (free end)	1.3°
Secondary cold-formed light steel beam and purlin	3°

The FEM of the 3D-Kagome truss core sandwich blast-resistant wall is shown in Figure 9, in which the angle ω between the truss core rod axis and the upper/lower panels is chosen as 54.7°; that is, $\sin\omega = \sqrt{2/3}$, the distance between the cells is 150 mm, same J-C material model is used, and all contact units are defined as "CONTACT AUTOMATIC SURFACE TO SURFACE".

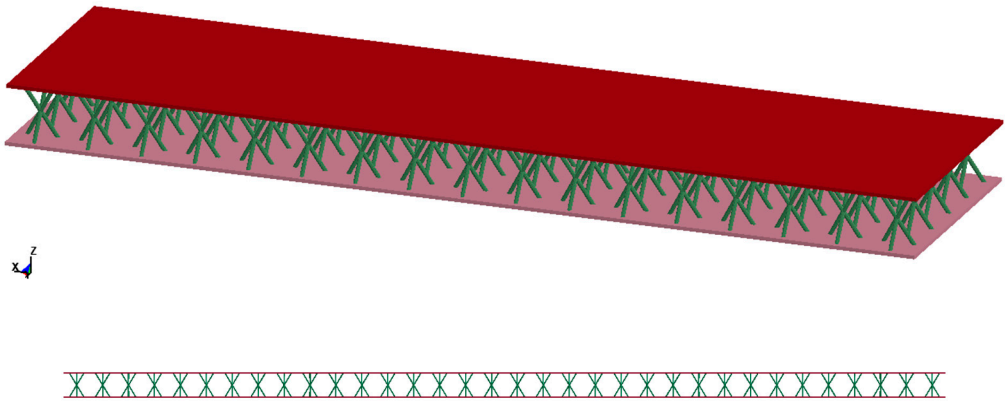

Figure 9. Quarter-scale model of a 3D-Kagome truss core sandwich blast-resistant wall. (The brown part is the upper or lower panel, and the green part is the truss core).

3.1. Influence Analysis of Radius of Truss Core Rod

According to Code for the Design of Blast-Resistant Control Building in the Petrochemical Industry (GB50779-2012) [5], 1 t TNT is chosen as the blast load, the blast distance is 30 m, the thickness of the sandwich blast-resistant wall is chosen as 150 mm, the thickness of the upper and lower panels H_f is 5 mm, and the radius R_c of the truss core rod changes from 2.5 mm to 9 mm. The plastic deformation energy curve of the truss core layer and the upper and lower panels for different truss core rod radii are shown in Figure 10. It is shown in Figure 8 that the main blast energy is absorbed by the truss core layer at first, and then the plastic deformation energy of the truss core layer is reduced with the increasing radius of the core layer rods. The plastic deformation energy of the upper panel and lower panels surpasses one of the truss core layers at the rod radius of 0.7 cm, which indicates that the stiffness of the core layer is too large to absorb energy effectively.

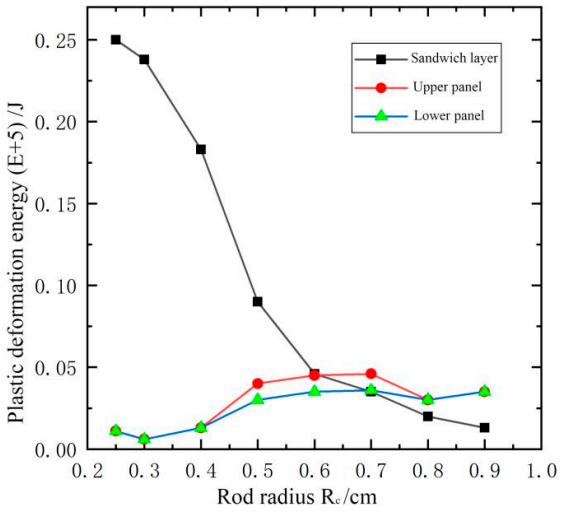

Figure 10. Plastic deformation energy with different bar radii.

The structural parameter ξ is defined as

$$\xi = \frac{\text{deformation energy of the truss core layer}}{\text{total deformation energy}} \tag{7}$$

The structural parameter ξ plays the role of the truss core layer in absorbing the blast energy, and the variation curve of parameter ξ for the different radii of the truss core rod is shown in Figure 11. It is shown in Figure 9 that the parameter ξ values are reduced from 0.93 to 0.88 when the radius values of the truss core rod are increased from 0.25 cm to 0.4 cm, which indicates that the blast energy is mainly dissipated by the plastic deformation of the core layer rod for the sandwich structure. However, the values of parameter ξ are reduced from 0.3 to 0.16 when the radius values of the truss core rod are increased from 0.7 cm to 0.9 cm, which indicates that the truss core layer does not dissipate the blast energy effectively.

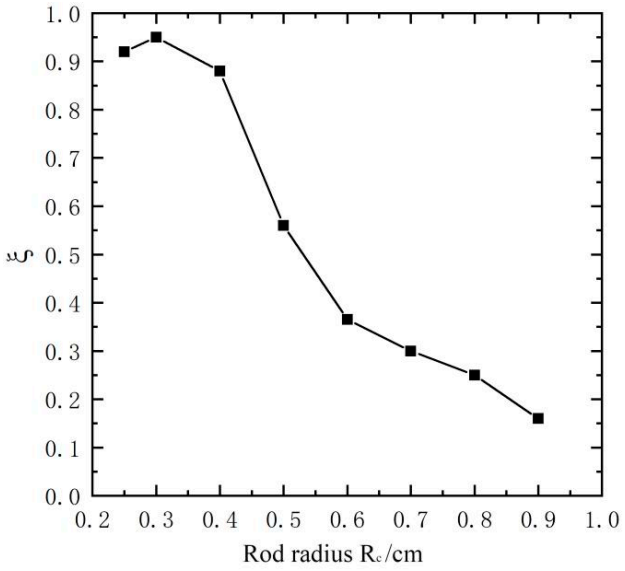

Figure 11. The structural parameter ξ with different bar radii.

The displacement response of the low panel with different truss core rod radii is shown in Figure 12. In Figure 12, it is shown that the out-of-plane displacement of the sandwich panel is reduced with the increase in the core rod radius, especially within the 0.2–0.4 cm

radius of the rod. When the radius of the truss core rod is 0.9 cm, the parameter ξ value is 0.16 in Figure 12, and it indicates that the plastic deformation energy of the truss core layer only accounts for 16% of the total plastic deformation energy of the sandwich blast-resistance wall. The out-of-plane displacement response of the sandwich blast-resistant wall is shown in Figure 13 for a 0.9 cm radius of the core rod, and it is clear that the panel of the sandwich blast-resistant wall becomes the main energy-consuming part.

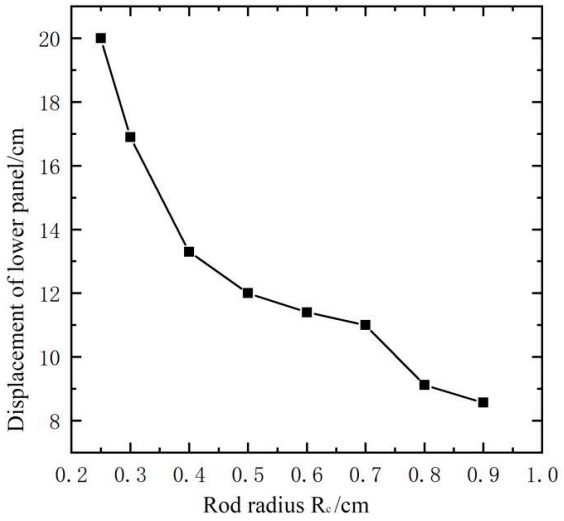

Figure 12. Displacement variation in lower panel with different bar radii.

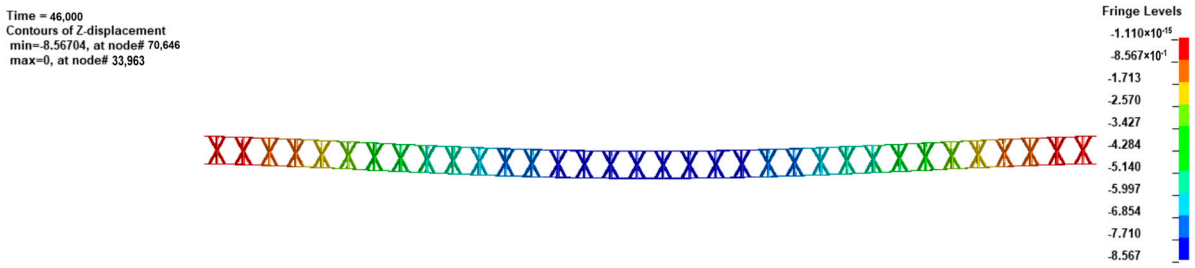

Figure 13. Displacement of the sandwich wall along Z-axis with 0.9 cm radius of the truss core rod.

3.2. Influence Analysis of Panel Thickness

It is shown that the parameter ξ value is reduced rapidly when the radius of the core rod is bigger than 0.5 cm in Figure 11. Assuming that the radius of the core rod is within 0.25–0.5 cm, the variation in the parameter ξ for different panel thicknesses of the sandwich blast-resistant wall is shown in Figure 14. When the panel thickness is 1 cm, the plastic deformation energy for different rod radii of the sandwich blast-resistant wall is shown in Figure 15.

In Figure 14, when the panel thickness is changed from 1 cm to 3 cm, the parameter ξ value is about 0.95 for 0.25 cm for the rod radius, 0.90 for 0.30 or 0.4 cm for the rod radius. In Figure 15, when the thickness of the panel is 1 cm, the plastic deformation energy curve of the sandwich blast-resistant wall has the same variation tendency as a 0.5 cm panel thickness. The plastic deformation energy of the truss core layer and the upper and lower panels are equal when the core rod radius is 0.8 cm.

When the thickness of the upper and lower panels is changed, the out-of-plane displacement of the center point of the lower panel for different rod radii is shown in Figure 16. For 1 cm panel thickness, the out-of-plane displacement of the center point of the lower panel for different core rod radii is shown in Figure 17.

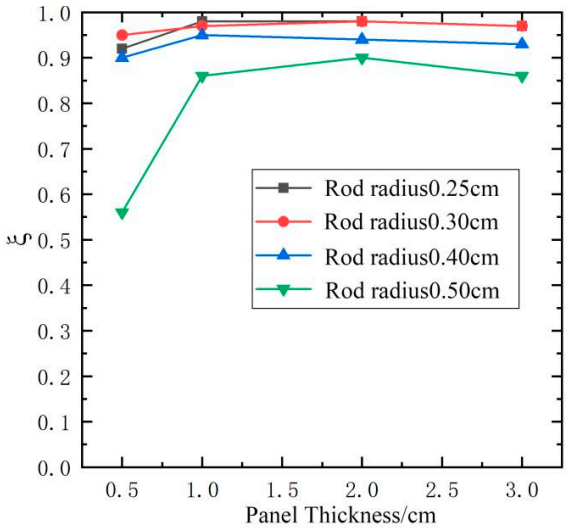

Figure 14. Parameter ξ for different panel thickness.

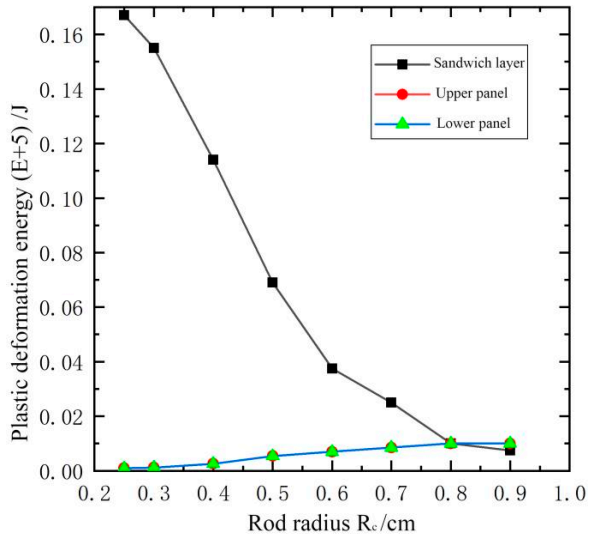

Figure 15. Plastic deformation energy for different rod radii.

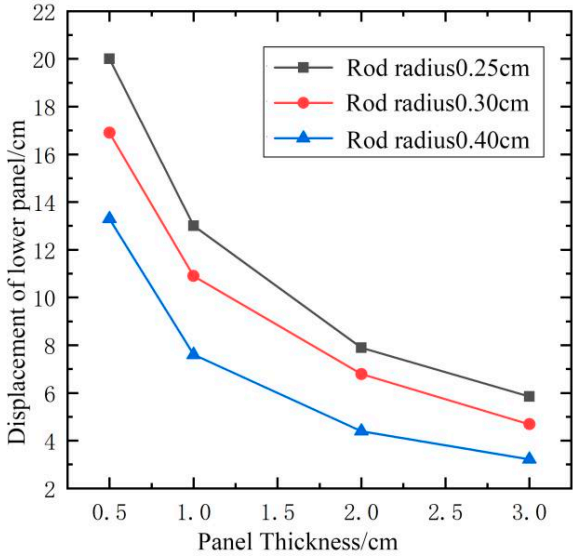

Figure 16. Displacement curves of lower panel with different panel thickness.

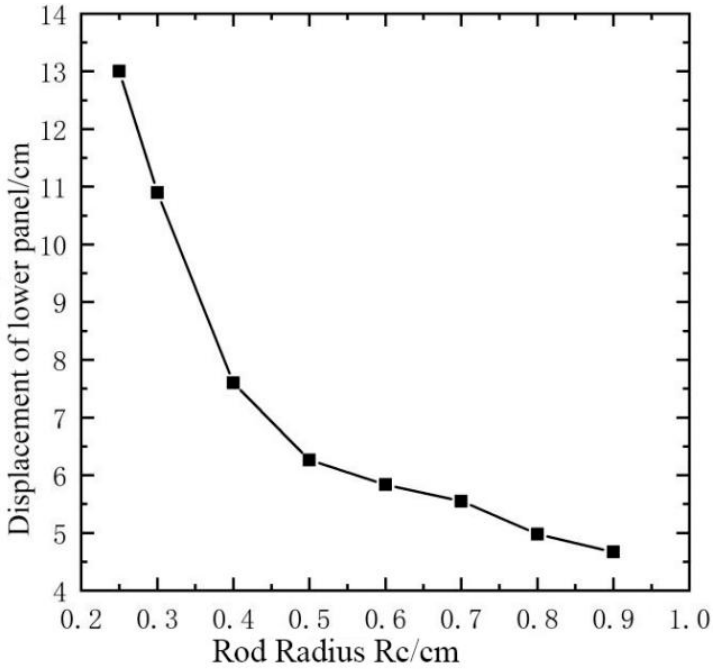

Figure 17. Displacement curves of lower panel with different rod radii.

It is observed from Figures 16 and 18 that the out-of-plane displacement of the center point of the lower panel is reduced rapidly when the panel thickness is increased from 0.5 cm to 3 cm and the core rod radius is increased from 0.25 cm to 0.4 cm. The out-of-plane displacement of the center point of the lower panel is 7.6 cm when the panel thickness is 1 cm, and the core rod radius is 0.4 cm; the corresponding displacement response history of the sandwich blast-resistance wall is shown in Figure 18, and the corresponding maximum θ = 1.71 is less than the normative allowable deformation value [θ]. It is observed from Figure 14 that the parameter ξ is 0.95 when the core rod radius is 0.4 cm, and the panel thickness is 1 cm. And the corresponding plastic deformation energy response history of the sandwich blast-resistant wall is shown in Figure 19. It is shown in Figure 19 that the dissipation energy ability of the truss core layer is much greater than that of the upper or lower panels. Therefore, it can be obtained that the optimal design parameters of the sandwich blast-resistance wall are 1 cm for the panel thickness and 0.4 cm for the core rod radius.

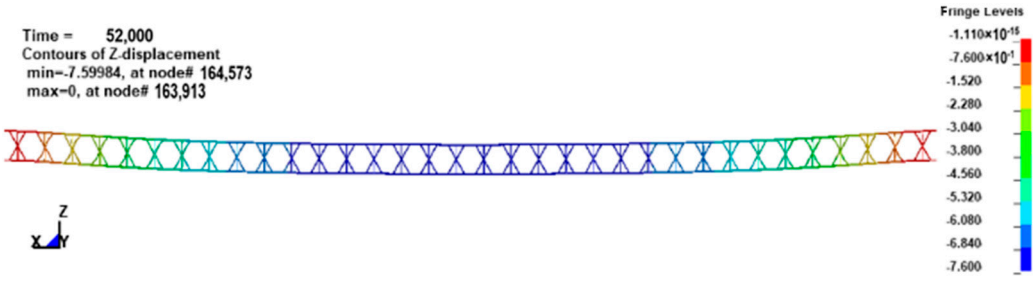

Figure 18. Out-of-plane displacement of the sandwich blast-resistant wall with 0.4 mm radius of the core rod.

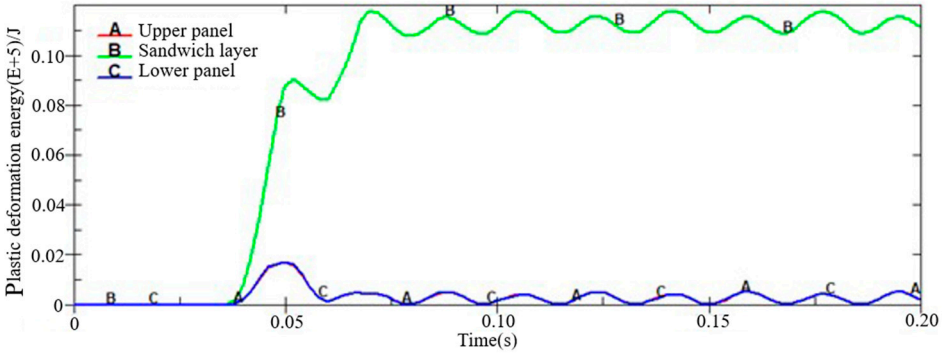

Figure 19. Plastic deformation energy time curve with 0.4 cm rod radius.

4. Results and Discussions

4.1. Assembly of Sandwich Blast-Resistant Wall

Based on the optimal design parameters of the sandwich blast-resistant wall, specifically a 1 cm panel thickness and 0.4 cm truss core rod radius, the optimal sandwich blast-resistant wall is assembled with a steel column of the petrochemical control structure and shown in Figure 20. Here, the connection between the wall and steel column in the finite element model is described using automatic face-to-face contact. The petrochemical control structural model with a 3D-Kagome sandwich blast-resistant wall is shown in Figure 21.

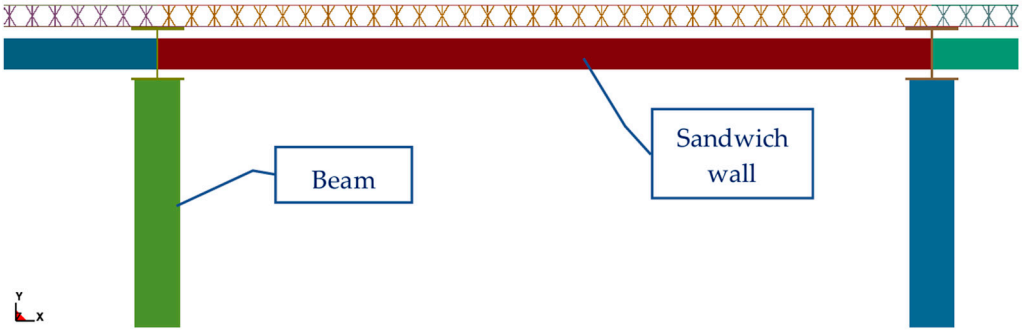

Figure 20. Connection between sandwich panel blast-resistant wall and steel columns (top view).

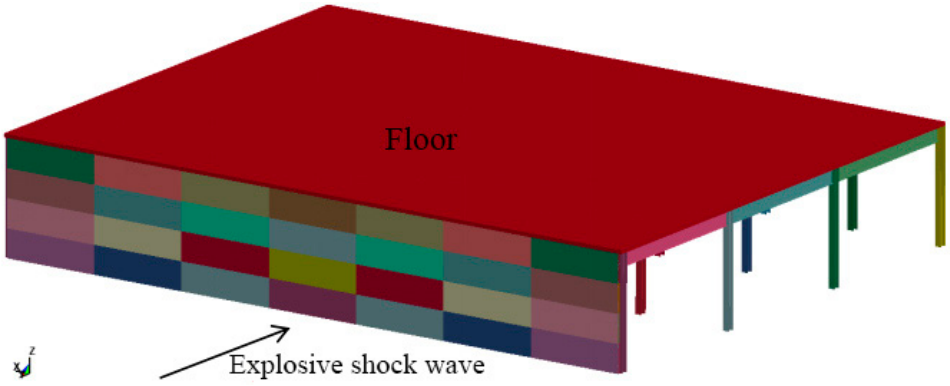

Figure 21. Petrochemical control structural model with 3D-Kagome sandwich blast-resistant wall.

In order to clearly describe the dynamic response of each sandwich blast-resistant wall under the blast load, the assembled blast-resistant walls are numbered to distinguish the location of the wall, and half of the whole wall model is shown in Figure 22.

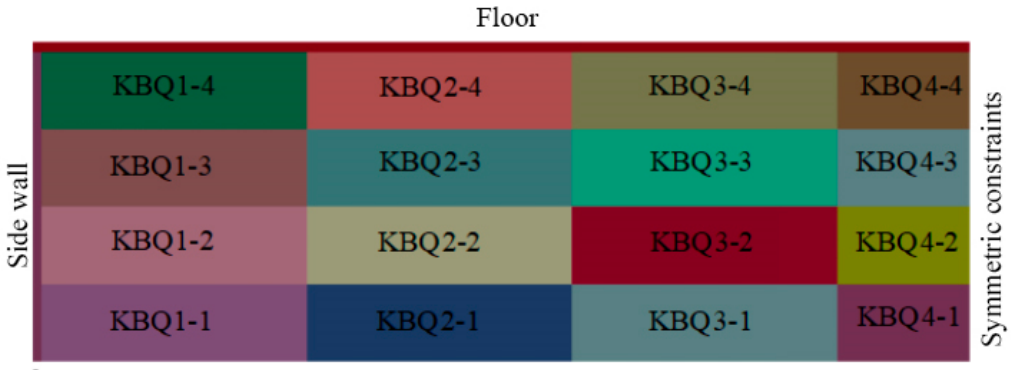

Figure 22. Sandwich blast-resistant walls number.

4.2. Dynamic Response Analysis

The value and location of the explosion load in this section satisfy the requirements of the "Code for design of blast-resistant control building in petrochemical industry" (GB50779-2012) [5], specifically, 1 ton TNT at 30 m blast distance from the control room structure. The specification establishes the criteria of a 30 m blast distance and a 1-ton TNT explosion mass with the integration of engineering safety principles and scientific research in explosion mechanics. The specified values reflect the explosion risks inherent to specific industrial sectors and have been validated to meet the stringent safety requirements for blast-resistant control buildings. Considering the solution time as 0.2 s, the displacement response clouds of the blast-front surface of the sandwich blast-resistant wall under the blast load are shown in Figure 23.

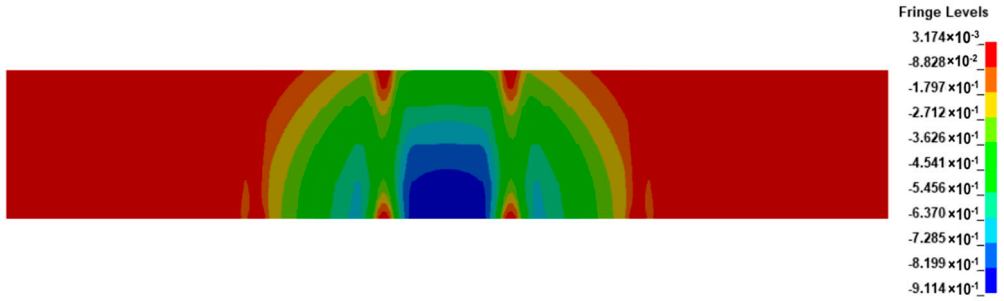

(**a**)

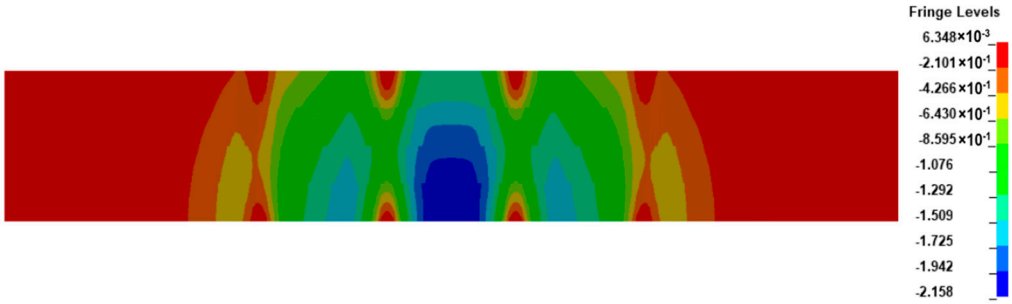

(**b**)

Figure 23. *Cont.*

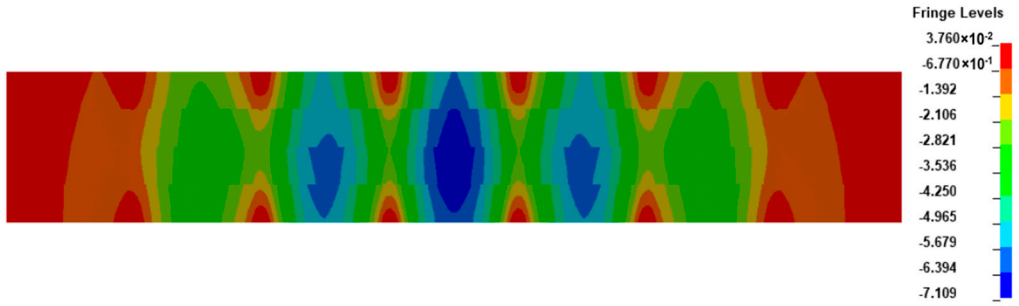

(**c**)

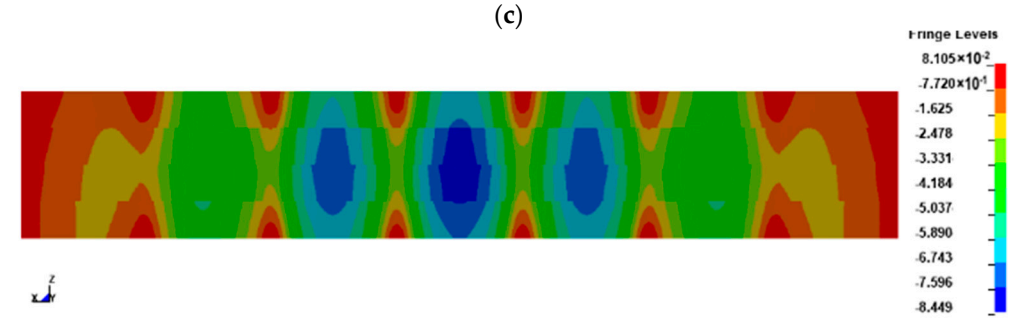

(**d**)

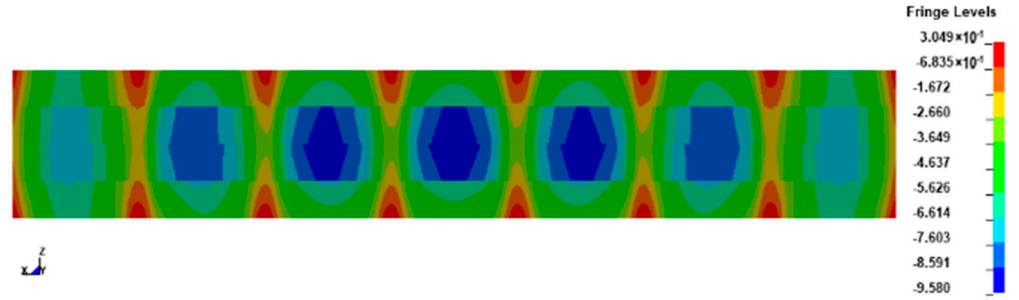

(**e**)

(**f**)

Figure 23. Displacement clouds of the blast-front surface of the truss core sandwich blast-resistant wall at different moments (cm): (**a**) t = 0.004 s; (**b**) t = 0.0046 s; (**c**) t = 0.05 s; (**d**) t = 0.054 s; (**e**) t = 0.062 s; and (**f**) t = 0.07 s.

In Figure 23, it can be observed that as the blast shock wave reaches the front wall of the petrochemical control structure under the blast load, the deformation of the sandwich blast-resistant wall (mainly KBQ4-1 and KBQ4-2) shown in Figure 23a occurs firstly near the center of the wall. In Figure 23b–f, with the increase in time, it has a larger deformation at the center span and extends to KBQ4-3, and the deformation near the center span of the blast wall also increases. Furthermore, the KBQ4-2 and KBQ4-3 walls produce the largest deformations, and the deformations of the KBQ4-1 and KBQ4-4 walls began to decrease. In general, the maximum deformation of the sandwich blast-resistant wall subjected to the blast load was observed to occur in the middle span of the wall. Smaller deformations

are observed at the two ends of the wall and at the connection parts between the wall and the column.

As it is known, the maximum displacement occurs in the middle span of the wall, then the lower panels of the KBQ4-2, KBQ4-3, KBQ3-2, and KBQ3-3 walls are selected, and the corresponding displacement response history is shown in Figure 24.

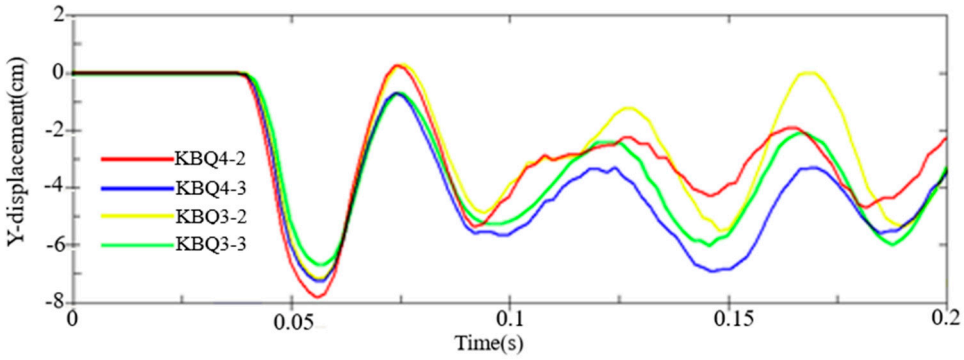

Figure 24. Lower panel displacement response of the center of sandwich blast-resistant wall.

In Figure 24, the maximum displacements of center points of the lower panels of the KBQ4-2, KBQ4-3, KBQ3-2, and KBQ3-3 walls are 7.89 cm, 7.3 cm, 7.1 cm, and 6.7 cm, respectively. Meanwhile, the rebound phenomenon of the lower panel appears after reaching the maximum deformation, and then reciprocal vibration occurs along the center point of the lower panel. The nature of reciprocal vibration is due to the action of the blast load being the instantaneous completion of the sandwich blast-resistant wall with inertial movement.

The displacement response clouds of the frame column under the blast load are shown in Figure 25, and the center point displacement response history of the middle span of the frame columns under the blast surface is shown in Figure 26. In Figure 25, it is evident that the location of the frame column plays a crucial role in its dynamic response. Specifically, the deformation initially manifests at the frame columns positioned on the explosion surface, denoted as A, B, C, and D, which serve as the corners of the blast-resistant face of the control room. Subsequently, it rapidly spreads to both sides. Finally, deformation also occurs at the frame column positioned on the back surface of the explosion. Notably, the frame column in the middle span of the explosion surface exhibits maximum deformation. Furthermore, Figure 26 illustrates the occurrence of a rebound phenomenon in the frame column.

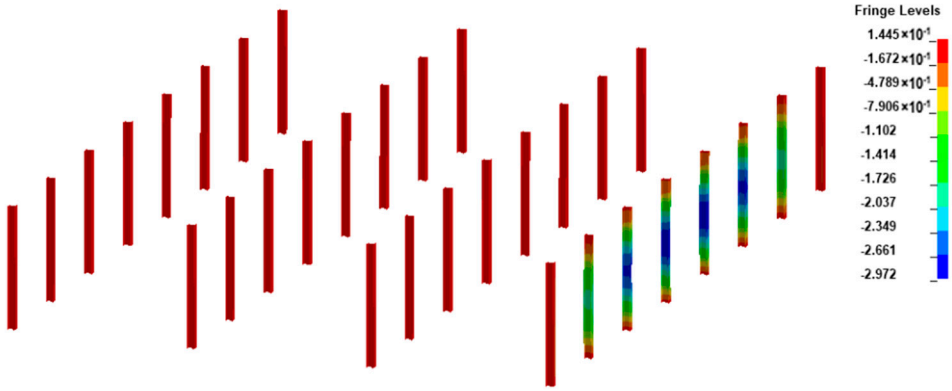

(**a**)

Figure 25. *Cont.*

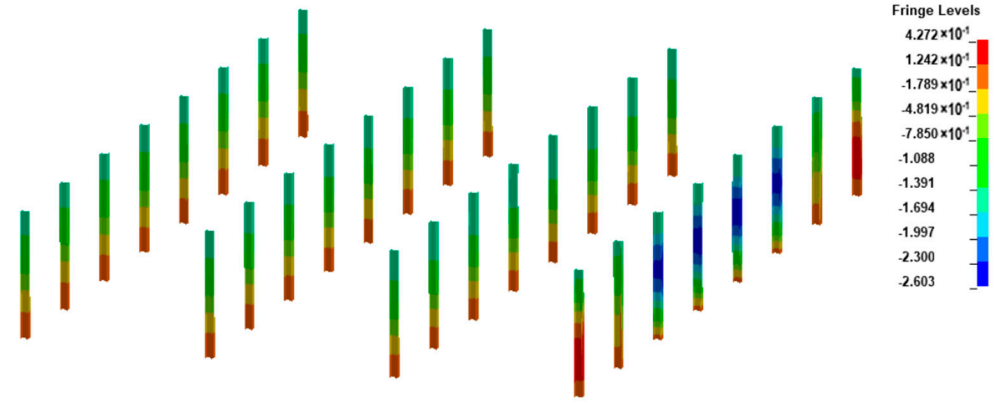

(**b**)

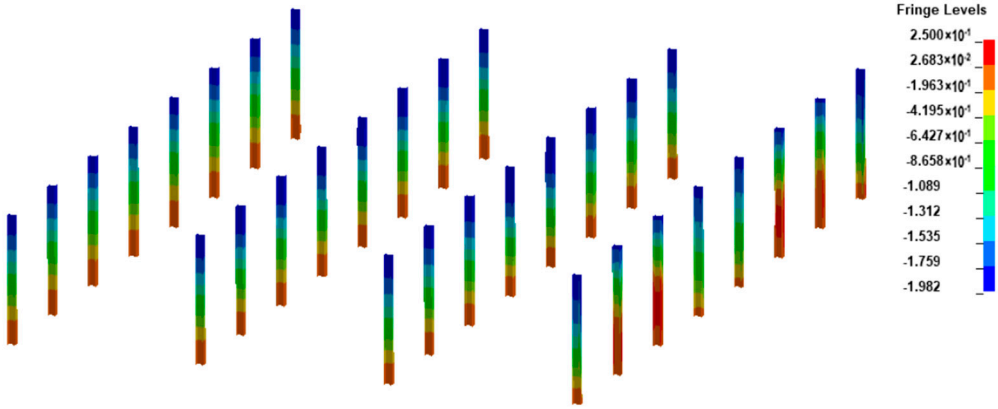

(**c**)

Figure 25. Y-directional displacement clouds of frame columns at different time instants: (**a**) t = 0.052 s; (**b**) t = 0.1 s; and (**c**) t = 0.182 s.

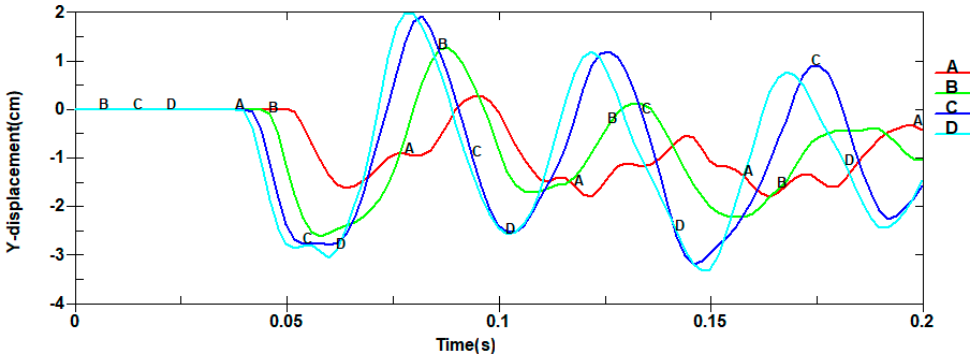

Figure 26. Displacement curve of the frame column of the control structure.

According to the Code for the design of a blast-resistant control building in the petrochemical industry (GB50779-2012) [5], the safety of the structural design is mainly measured by the allowable deformation of each member of the structure subjected to the explosive load. In this paper, the support angle was used as the main measure criterion. The above modeling and solution by finite element software were used to obtain the dynamic response of the structure of 1 ton TNT at a blast distance of 30 m. Through the calculation, the center points maximum displacement and the bearing angle of the sandwich blast-resistant walls at different locations of the blast surface are shown in Table 7, and the maximum deformation and bearing angle of the frame column are shown in Table 8.

Table 7. Center point displacement and bearing angle of sandwich blast-resistant walls.

Blast-Resistant Wall Number	Y-Deformation (Δ/*m*)	Corner (*θ*/°)	Blast-Resistant Wall Number	Y-Deformation (Δ/*m*)	Corner (*θ*/°)
KBQ1-1	0.055	1.24	KBQ3-1	0.063	1.42
KBQ1-2	0.058	1.30	KBQ3-2	0.071	1.59
KBQ1-3	0.060	1.35	KBQ3-3	0.067	1.50
KBQ1-4	0.054	1.21	KBQ3-4	0.061	1.37
KBQ2-1	0.055	1.24	KBQ4-1	0.070	1.57
KBQ2-2	0.062	1.39	KBQ4-2	0.079	1.77
KBQ2-3	0.064	1.44	KBQ4-3	0.073	1.64
KBQ2-4	0.052	1.17	KBQ4-4	0.068	1.53
Scope	0.052–0.064	1.17–1.44		0.061–0.079	1.37–1.77

Table 8. Maximum deformation and bearing angle of the frame column.

Frame Column Number	Y-Directional Deformation (Δ/*m*)	Corner (*θ*/°)
KZA	0.017	0.32
KZB	0.027	0.52
KZC	0.031	0.60
KZD	0.033	0.63
Scope	0.017–0.033	0.032–0.063

It is clear from Tables 7 and 8 that deformations for different parts of the sandwich blast-resistant walls and frame column are smaller than the allowable values of the petrochemical control structural design code.

5. Conclusions

This paper focuses on studying the blast-resistant performance of a control room subjected to vapor cloud explosion load in the petrochemical industry. The blast-resistant performance of the steel control room with an assembled 3D-Kagome sandwich blast-resistant wall is investigated using the finite element analysis method. This study includes numerical modeling of the control room structure, the optimal blast-resistant design of the 3D-Kagome sandwich blast-resistant wall, and dynamic response analysis of the control room structure. Increasing the diameter of the core layer rods leads to a continuous decrease in the plastic deformation energy of the core layer, while that of the upper and lower panels continues to increase. When the rod radius is too large, the upper and lower panels become the main energy-absorbing components of the sandwich blast-resistant wall. Increasing the thickness of the upper and lower panels initially improves the plastic deformation energy of the core layer. The plastic deformation energy of the core layer accounts for approximately 90% of the total, indicating that excessively thick panels do not significantly enhance the blast-resistant performance of the sandwich wall. When the rod radius of the sandwich layer is 4 mm, the thickness of the upper/lower panel is 10 mm, the plastic deformation energy of the sandwich layer accounts for 93% of the total. Additionally, the displacement at the center point of the lower panel meets the specified deformation requirements. For the assembly of the blast-resistant wall subjected to a 1-ton TNT explosion at a distance of 30 m, it experiences the highest displacement in the center of the blast wall. The maximum displacements at the center point of the lower panel for blast-resistant walls KBQ4-2, KBQ4-3, KBQ3-2, and KBQ3-3 are 7.89 cm, 7.3 cm, 7.1 cm, and 6.7 cm, respectively. The displacement in the center spreads in a hemispherical manner to both sides.

In order to guarantee computation accuracy, two available blast experimental data of the truss core sandwich panel and steel one are used to validate the finite element modeling methods by comparing them. The comparison results between simulation and experiment methods show that the error is within 1.25–6.63%, which shows a good agreement between them.

The proposed design method, while aiming to enhance the sustainability of the petrochemical control room, comes with potential drawbacks that could impact both its implementation and long-term performance. Introducing a truss core layer may result in stiffness discrepancies, leading to uneven structural responses. The intricate fabrication of the sandwich panel poses challenges, potentially raising production costs due to manufacturing complexity. Maintenance and repair difficulties, especially in accessing small elements, are anticipated due to the structural complexity introduced by the truss core layer. These considerations emphasize the importance of careful evaluation and mitigation strategies in implementing this design method. In response to these challenges, comprehensive design optimization is crucial for achieving the superior blast resistance of the petrochemical control room structures in future research.

Author Contributions: Conceptualization, Z.L. and D.C.; methodology, Z.L.; software, D.C.; validation, D.C. and Y.J.; formal analysis, D.C.; investigation, X.L.; resources, X.D.; data curation, Y.J.; writing—original draft preparation, X.D.; writing—review and editing, X.D.; visualization, Y.J.; supervision, X.L.; project administration, Z.L.; funding acquisition, Z.L. All authors have read and agreed to the published version of the manuscript.

Funding: This work was supported by the Key Technology Research and Development Program of Shaanxi Province of China under grant number 2024GX-YBXM-235.

Data Availability Statement: Data are contained within the article.

Conflicts of Interest: The authors declare no conflict of interest.

References

1. Oran, E.S.; Chamberlain, G.; Pekalski, A. Mechanisms and occurrence of detonations in vapor cloud explosions. *Prog. Energy Combust. Sci.* **2020**, *77*, 100804. [CrossRef]
2. Korea Times. 4 Dead, 4 Injured in Factory Explosion in Yeosu. The Korea Times. Available online: https://www.koreatimes.co.kr/www/nation/2022/02/251_323715.html (accessed on 25 February 2022).
3. Chang, W.; Xiong, Y. Fire at Shanghai Petrochemical Complex Kills at Least One Person. CNN. Available online: https://www.cnn.com/2022/06/17/china/shanghai-petrochemical-fire-death-intl-hnk/index.html (accessed on 18 June 2022).
4. Malay Mail. Explosion Reported at Sabah-Sarawak Gas Pipeline in Lawas, One Fatality. Malay Mail. Available online: https://www.malaymail.com/news/malaysia/2022/11/16/explosion-reported-at-sabah-sarawak-gas-pipeline-in-lawas-one-fatality/40047 (accessed on 16 November 2022).
5. GB50779—2012. Standardization Administration of China. Code for Design of Blast Resistant Control Building in Petrochemical Industry. China Planning Press: Beijing, China, 2012. (In Chinese)
6. 14J938. Standardization Administration of China. Blast-Resistant and Pressure-Relief Doors; Windows; Roofs; and Wall Structures. China Academy of Building Research:: Beijing, China, 2014. (In Chinese)
7. ASCE. *Design of Blast Resistant Buildings in Petrochemical Facilities*, 2nd ed.; ASCE: Reston, VA, USA, 2010.
8. Pritchard, D.; Roberts, A. Blast effects from vapour cloud explosions: A decade of progress. *Saf. Sci.* **1993**, *16*, 527–548. [CrossRef]
9. Clubley, S.K. Non-linear long duration blast loading of cylindrical shell structures. *Eng. Struct.* **2014**, *59*, 113–126. [CrossRef]
10. Li, B.; Pan, T.C.; Nair, A. A case study of the effect of cladding panels on the response of reinforced concrete frames subjected to distant blast loadings. *Nucl. Eng. Des* **2009**, *239*, 455–469. [CrossRef]
11. Louca, L.; Boh, J.; Choo, Y. Design and analysis of stainless steel profiled blast barriers. *J. Constr. Steel Res.* **2004**, *60*, 1699–1723. [CrossRef]
12. Boh, J.; Louca, L.; Choo, Y. Energy absorbing passive impact barrier for profiled blastwalls. *Int. J. Impact Eng.* **2005**, *31*, 976–995. [CrossRef]
13. Ambrosini, D.; Luccioni, B.M. Reinforced concrete wall as protection against accidental explosions in the petrochemical industry. *Struct. Eng. Mech.* **2009**, *32*, 213–233. [CrossRef]
14. Kiakojouri, F.; De Biagi, V.; Chiaia, B.; Sheidaii, M.R. Strengthening and retrofitting techniques to mitigate progressive collapse: A critical review and future research agenda. *Eng. Struct.* **2022**, *262*, 114274. [CrossRef]
15. Kiakojouri, F.; De Biagi, V.; Chiaia, B.; Sheidaii, M.R. Progressive collapse of framed building structures: Current knowledge and future prospects. *Eng. Struct.* **2020**, *206*, 110061. [CrossRef]
16. Winget, D.G.; Marchand, K.A.; Williamson, E.B. Analysis and Design of Critical Bridges Subjected to Blast Loads. *J. Struct. Eng.* **2005**, *131*, 1243. [CrossRef]
17. Nguyen, T.; Kim, S. Lattice Structures for Lightweight and High-Strength Architectural Applications. *Adv. Eng. Mater.* **2020**, *22*, 2000294.

18. Harper, C.A.; Franklin, S. Durability and Risks of Metal Core Sandwich Panels under Industrial Conditions. *J. Build. Eng.* **2022**, *35*, 101892.
19. Watson, A.; Moriarty, P. Applications of Hybrid Sandwich Panels in Aerospace and Automotive Industries. *Compos. Part B Eng.* **2021**, *212*, 108678.
20. Zhang, Y.; Wang, L. Performance Analysis of Structural Panels under Blast Loading. *Int. J. Impact Eng.* **2019**, *133*, 103312.
21. Vaziri, A.; Xue, Z.; John, W. Performance and failure of metal sandwich plates subjected to shock loading. *J. Mech. Mater. Struct.* **2007**, *2*, 1947–1963. [CrossRef]
22. Jin, N.; Wang, F.; Wang, Y.; Zhang, B.; Cheng, H.; Zhang, H. Effect of structural parameters on mechanical properties of Pyramidal Kagome lattice material under impact loading. *Int. J. Impact Eng.* **2019**, *132*, 103313. [CrossRef]
23. Zhang, G.; Wang, B.; Ma, L.; Xiong, J.; Wu, L. Response of sandwich structures with pyramidal truss cores under the compression and impact loading. *Compos. Struct.* **2013**, *100*, 451–463. [CrossRef]
24. Kemerli, U.; Kahveci, K. Conjugate forced convective heat transfer in a sandwich panel with a Kagome truss core: The effects of strut length and diameter. *Appl. Therm. Eng.* **2020**, *167*, 114794. [CrossRef]
25. Varghese, R.M.; Varghese, M.K. Comparative study on the blast load response of woven and lattice core metallic sandwich panels. *Mater. Today Proc.* **2022**, *65*, 1343–1347. [CrossRef]
26. Xu, L.; Ruan, Q.; Shen, Q.; Xi, L.; Gao, J.; Li, Y. Optimization Design of Lattice Structures in Internal Cooling Channel with Variable Aspect Ratio of Gas Turbine Blade. *Energies* **2021**, *14*, 3954. [CrossRef]
27. Wadley, H.N.G.; Fleck, N.A.; Evans, G.A. Fabrication and structural performance of periodic cellular metal sandwich structures. *Compos. Sci. Technol.* **2003**, *63*, 2331–2343. [CrossRef]
28. Dharmasena, K.P.; Wadley, H.N.G.; Williams, K.; Xue, Z.; Hutchinson, J.W. Response of Metallic Pyramidal Lattice Core Sandwich Panels to High Intensity Impulsive Loading in Air. *Int. J. Impact Eng.* **2011**, *38*, 275–289. [CrossRef]
29. Zhao, P.; Zhang, P.; Zhang, L.; Wang, Z.; Wang, Q.; Xu, Y. Experimental study on blast-resistant performance of polyurea coated steel plate structure. *J. Beijing Univ. Technol.* **2018**, *38*, 118–123. (In Chinese)
30. Johnson, G.R.; Cook, W.H. A Constitutive Model and Data for Metals Subjected to Large Strains, High Strain Rates, and High Temperatures. In Proceedings of the 7th International Symposium on Ballistics, The Hague, The Netherlands, 19–21 April 1983.
31. Johnson, G.R.; Cook, W.H. Fracture Characteristics of Three Metals Subjected to Various Strains, Strain Rates, Temperatures and Pressures. *Eng. Fract. Mech.* **1985**, *21*, 31–48. [CrossRef]